Rare Metal Materials and Engineering
Volume 51, Issue 5, May 2022
Available online at www.rmme.ac.cn

Science Press

Cite this article as: Yuan Zengyin, Wang Youbin, Zou Rui, et al. Effect of LDHs on Corrosion Behavior of 6061Al Alloy in NaCl Solution with Different Dissolved Oxygen Contents[J]. Rare Metal Materials and Engineering, 2022, 51(05): 1589-1596.

ARTICLE

Effect of LDHs on Corrosion Behavior of 6061Al Alloy in NaCl Solution with Different Dissolved Oxygen Contents

Yuan Zengyin[1,2], Wang Youbin[1,2], Zou Rui[1,2], Yang Yuancheng[1,2], Fujita Toyohisa[1,2], Wei Yuezhou[1,2]

[1] Guangxi Key Laboratory of Processing for Non-ferrous Metal and Featured Materials, Nanning 530004, China; [2] School of Resources, Environment and Materials, Guangxi University, Nanning 530004, China

Abstract: The layered double hydroxides (LDHs) were prepared on 6061Al alloy by in-situ synthesis. The effects of LDHs on the corrosion behavior of 6061Al alloy in 3.5wt% NaCl solution with different dissolved oxygen (DO) contents (1~16 mg/L) were analyzed through the polarization curves (Tafel) and electrochemical impedance spectroscopy (EIS). The results indicate that the polarization processes of 6061Al and LDHs/6061Al alloys are controlled by DO diffusion. With increasing the DO content, a large number of pits appear on the 6061Al alloy surface, and the pit is gradually deepened. The corrosion current is increased from 1.273 μA to 1.743 μA, and the pit depth is increased from 12 μm to 19 μm. However, no pits can be observed in LDHs/6061Al alloy at different DO contents, which is attributed to the inhibition of DO diffusion and the polarization process. In addition, the resistance of 6061Al alloy is increased with increasing the DO content, which is related to the formation of Al_2O_3. However, the resistance of LDHs/6061Al alloy has no obvious change at different DO contents, showing excellent isolation performance against DO.

Key words: LDHs; dissolved oxygen; aluminum alloy; corrosion

The 6061Al alloy is a heat-treated aluminum alloy with excellent processing properties and good mechanical properties, which has been widely used for shipbuilding, marine equipment, transportation, and other industries[1]. However, 6061Al alloy is prone to corrosion in harsh marine environment, resulting in a significant decline in service life[2]. The corrosion process of aluminum alloy is accompanied by the anodic dissolution and cathodic oxygen reduction. Dissolved oxygen (DO) and corrosive ions (Cl^-) in seawater have a great impact on the electrochemical corrosion behavior of aluminum alloy[3].

In recent years, the effect of DO on the corrosion behavior of metal attracts widespread attention. Dexter et al[4] found that the corrosion potential of pure aluminum and 5052Al alloy is positively shifted with increasing the DO content. Shi et al[5] studied the effect of oxygen content on the galvanic corrosion kinetics of Al2024/Q235/304L alloy, and found that the anodic corrosion rate is increased with increasing the oxygen content. Su et al[6] found that DO can accelerate the cathodic process and inhibit the anodic process of low alloy steel under hydrostatic pressure.

To slow down the corrosion of aluminum alloy in seawater, a series of surface treatment techniques, such as anodic oxidation, electroplating, and spraying, have been adopted for corrosion protection[7,8]. The corrosion resistance of aluminum alloy can be effectively enhanced by preparing various films or coatings on the surface of aluminum alloy. Among these films or coatings, the excellent corrosion resistance of layered double hydroxides (LDHs) attracts extensive attention[9].

LDHs are the environmentally-friendly material, which can be used as the protection film to inhibit the corrosion of aluminum alloy. At present, the principle of the corrosion resistance of LDHs is still ambiguous. It is proved that LDHs have a trapping effect on Cl^-, and can prevent further corrosion by fixing Cl^- between layers[10,11]. However, the inhibitory effect of LDHs on DO is rarely discussed. At present, there are many preparation methods of LDHs, such as in-situ synthesis[12,13], coprecipitation[14,15], layer by layer

Received date: June 30, 2021
Foundation item: National Natural Science Foundation of China (11975082); Guangxi Science and Technology Major Project (AA17204100)
Corresponding author: Wang Youbin, Ph. D., Lecturer, Guangxi Key Laboratory of Processing for Non-ferrous Metal and Featured Materials, Guangxi University, Nanning 530004, P. R. China, Tel: 0086-771-3224332, E-mail: wangyoubin@gxu.edu.cn

assembly[16,17], hydrothermal deposition[18], and electrochemical deposition[19,20]. The in-situ synthesis method has the advantages of easy operation and good combination of film and substrate.

In this research, LDHs were prepared on the surface of 6061Al alloy by in-situ synthesis. Different DO contents (1~16 mg/L) were used according to the distribution of DO in marine environment[21,22]. The effect of LDHs on the corrosion behavior of 6061Al alloy in NaCl solution with different DO contents was studied using electrochemical testing techniques. In addition, the results provide a supplementary explanation for the excellent corrosion resistance of LDHs.

1 Experiment

The ultra-pure water with a resistivity greater than 18 MΩ·cm was used in this research. All reagents were directly used without further purification. The 6061Al alloy (0.15wt%~0.4wt% Cu, 0.15wt% Mn, 0.80wt%~1.2wt% Mg, 0.25wt% Zn, 0.4wt%~0.8wt% Si, 0.15wt% Ti, and balanced Al) was cut into specimens with the size of *Φ*14 mm×5 mm, and then polished with silicon carbide sandpaper of 320#, 600#, 1200#, and 2000# and by diamond of 0.1 μm in size.

LDHs were prepared by conventional in-situ synthesis method[23]. The 0.03 mol/L $CO(NH_2)_2$ and 0.005 mol/L $Zn(NO_3)_2$ were dissolved in 500 mL ultrapure water, and the pH value was adjusted to neutral with 5vol% diluted ammonia. Then the specimens were placed in the solution and kept in a water bath at 80 °C for 4 h. After the hydrothermal treatment, the specimen was taken out, washed with pure water and ethanol repeatedly, and then dried. The untreated specimens were named as 6061Al alloy, and the specimens after in-situ synthesis were named as LDHs/6061Al alloy.

X-ray diffraction (XRD, D/MAX 2500 V, Rigaku, Japan) was used to analyze the crystal structure of the films. The monochromator was operated at 40 kV and 150 mA. The scanning rate was 8°/min. The surface and cross-section morphology characteristics of LDHs/6061Al alloy were studied by scanning electron microscope (SEM, SU8220, Hitachi, Japan). The elements of LDHs/6061Al alloy films were measured by energy disperse spectroscopy (EDS, QUANTAX, Bruker, Germany). The corrosion morphology was characterized by optical microscope (OM, DVM6s, Leica, Germany) and SEM (Pro X, Phenom, Netherlands). Moreover, Fourier transform infrared spectroscopy (FTIR, IRTracer-100, Shimadzu, Japan) was used to analyze the molecular structure and chemical bond.

The electrochemical experiments were conducted to study the influence of different DO contents on the corrosion behavior of LDHs/6061Al and 6061Al alloys. The schematic diagram of the determination device is shown in Fig. 1. The three-electrode system was adopted in the experiment: the specimen, platinum sheet, and saturated calomel electrode were working electrode, counter electrode, and reference electrode, respectively. The working electrode was encapsulated with epoxy resin, and the reaction area of 1 cm^2 was reserved. All experiments were conducted on the electrochemical workstation (1010A, Gamry, USA) in 3.5wt% NaCl solution. The DO content was determined by DO analyzer (J650s, LeiCi, China).

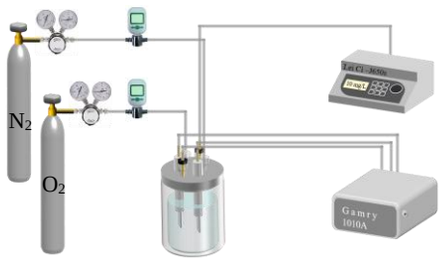

Fig.1 Schematic diagram of experiment device

To obtain the stable open circuit potential, the solution was placed still for 30 min before each measurement. The electrochemical resistance spectroscopy (EIS) and Tafel polarization curves were measured at different DO contents (1~16 mg/L), and three measurements were performed at each DO content to ensure the accuracy. The polarization curve was tested with a potential scanning rate of 5 mV/s under the scanning range from −1.0 V vs. SCE to 0 V vs. SCE. EIS was tested with the amplitude of 10 mV under the frequency from 10^5 Hz to 10^{-2} Hz. The potential amplitude of 6061Al and LDHs/6061Al alloys was 5 and 10 mV, respectively[24]. Before EIS tests, the solution was placed in the electrolytic cell for 600 s to obtain a stable open circuit potential.

2 Results and Discussion

2.1 Structure and morphology of LDHs/6061Al alloy

XRD patterns of 6061Al and LDHs/6061Al alloy are shown in Fig. 2. It can be seen that there are Al and Mg_2Si phases in 6061Al alloy.

XRD results of LDHs/6061Al alloy films show the characteristics of hydrotalcite type clay, corresponding to the typical diffraction peaks of (003), (006), and (100) planes[25]. The calculated crystal plane spacing $d_{(003)}$ is 0.76 nm, which is consistent with Ref.[26]. The lattice constant can be calculated as $a=b=2d_{(110)}$=0.3072 nm, which is consistent with the results in Ref. [27, 28]. These results all suggest that LDHs are successfully prepared on 6061Al alloys.

Fig. 3 shows FTIR spectrum of LDHs/6061Al alloy. The broadband centered at 3440 cm^{-1} corresponds to the O-H

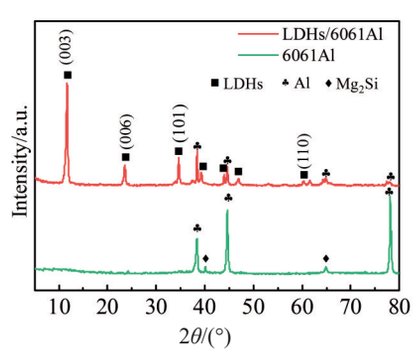

Fig.2 XRD patterns of 6061Al and LDHs/6061Al alloys

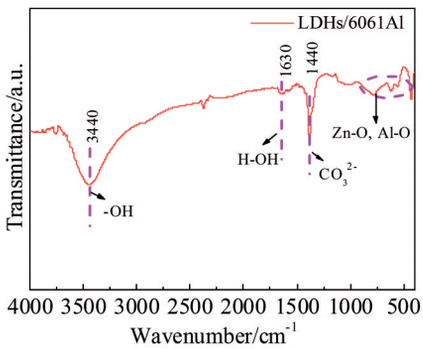

Fig.3 FTIR spectrum of LDHs/6061Al alloy

stretching vibration of the -OH group and interlayer H_2O molecule. The weak peak at 1630 cm^{-1} corresponds to the interlayer H_2O molecule. The strong peak at 1385 cm^{-1} corresponds to the C-O tensile vibration of interlayer carbonate in LDHs/6061Al alloy. A series of peaks centered below 1000 cm^{-1} are due to the stretching and bending of metal-oxygen (Zn-O, Al-O)[29,30].

SEM images and EDS analysis of LDHs/6061Al alloy are shown in Fig. 4. LDHs film with the thickness of tens of nanometers is composed of hexagonal nanosheets of different sizes (2~5 μm). The film grows perpendicularly to 6061Al alloy substrate, presenting an obvious orientation relationship. The surface of 6061Al alloy substrate is completely covered by LDHs, and there is no phenomenon of aggregation growth. Fig. 4c shows the cross-sectional morphology of the LDHs/6061Al alloy. The LDHs film has no breakpoint and shows the height inhomogeneity, indicating that the film is well bonded with the substrate with an average film thickness of 3.2 μm. Fig. 4d shows EDS results of point A in Fig. 4b. The atomic ratio of Zn/Al in LDHs/6061Al alloy is 1.93, which is basically consistent with Ref.[31].

2.2 Formation mechanism of LDHs

The schematic diagram of in-situ synthesis process of LDHs/6061Al alloy is shown in Fig.5, and Eq.(1~7) show the reactions during the process, as follows:

$$CO(NH_2)_2+3H_2O\rightarrow 2NH_4^++2OH^-+CO_2\uparrow \quad (1)$$

$$Al_2O_3+2OH^-+3H_2O\rightarrow 2Al(OH)_4^- \quad (2)$$

$$Al\rightarrow Al^{3+}+3e^- \quad (3)$$

$$O_2+H_2O+4e^-\rightarrow 4OH^- \quad (4)$$

$$Zn^{2+}+OH^-\rightarrow Zn(OH)^+ \quad (5)$$

$$Al_2O_3+3H_2O\rightarrow 2Al(OH)_3 \quad (6)$$

$$Al(OH)_3+2Zn(OH)^++H_2O+CO_3^{2-}\rightarrow ZnAl\text{-}LDHs \quad (7)$$

The hydrolysis of urea produces CO_2 and OH^- (Eq.(1)) and CO_2 dissolves in water to form CO_3^{2-}, which then acts as the interlayer anion to balance the charge in subsequent reactions[32]. The OH^- reacts with Al_2O_3 on the 6061Al substrate to form $Al(OH)_4^-$ (Eq. (2)), leading to the partial rupture of the Al_2O_3 film, which then causes the substrate to contact with the solution. Thus, the 6061Al substrate dissolves, forming more Al^{3+} (Eq. (3)). The O_2 is reduced to OH^- (Eq. (4)), thereby increasing the local alkalinity. The alkaline environment provides enough OH^- for Zn^{2+} to form $Zn(OH)^+$ (Eq. (5)). Besides, $Al(OH)_3$ is formed by the hydration of Al_2O_3 (Eq.(6)), and the Zn^{2+} in $Zn(OH)^+$ enters the layer of $Al(OH)_3$ and occupies some Al^{3+} sites[33]. Therefore, ZnAl-LDHs gradually form based on $Al(OH)_3$ (Eq.(7)).

2.3 Polarization behavior of LDHs

The cathodic polarization is widely used to study the polarization behavior of films. Fig. 6 shows the cathodic polarization curve of 6061Al and LDHs/6061Al alloys in 3.5wt% NaCl solution with different DO contents.

With increasing the DO content, the corrosion potential E_{corr}

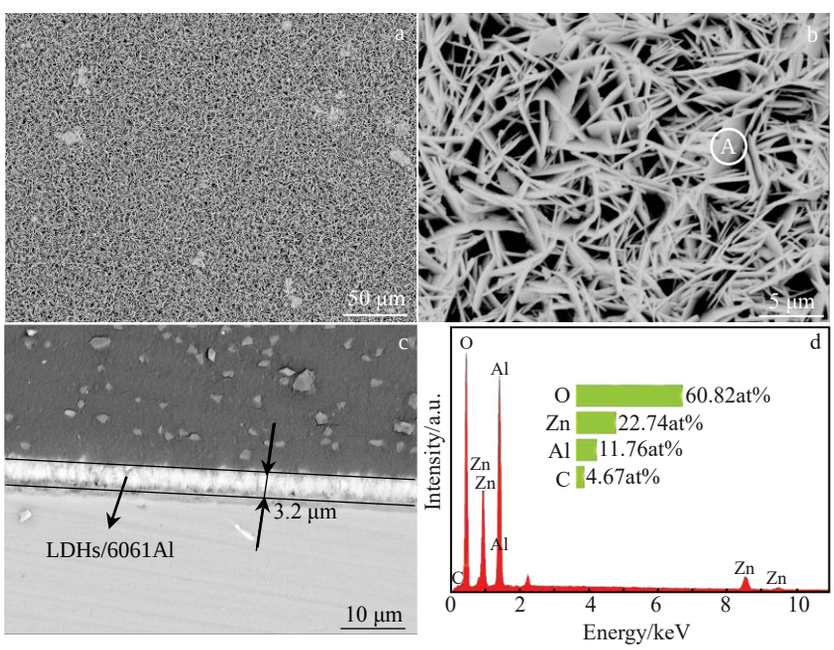

Fig.4 SEM surface (a, b) and cross-section (c) morphologies and EDS analysis of point A in Fig.4b (d) of LDHs/6061Al alloy

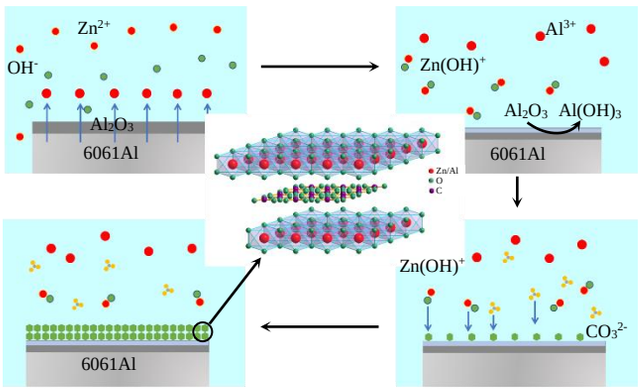

Fig.5 Schematic diagram of in-situ synthesis process of LDHs film on 6061Al alloy substrate

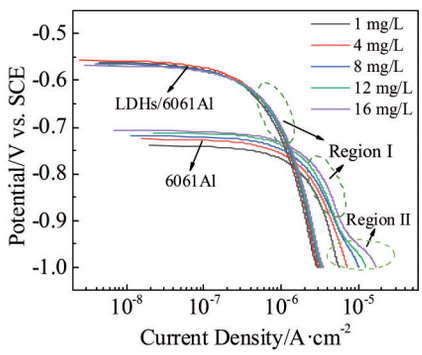

Fig.6 Cathodic polarization curves of 6061Al and LDHs/6061Al alloys in 3.5wt% NaCl solution with different DO contents

of 6061Al alloy is increased, while that of LDHs/6061Al alloy does not change significantly, indicating that LDHs show an effective inhibitory effect against DO. The cathodic polarization curves of LDHs/6061Al alloy shift towards the region of low current density, and the corrosion potential also moves towards the positive direction. At the same potential, the current of LDHs/6061Al alloy is obviously less than that of 6061Al alloy, which indicates that the LDHs film enhances the corrosion resistance of 6061Al alloy substrate.

Tafel slope can be used to judge the initiation difficulty of electrode reaction. The larger the slope, the greater the resistance against the electrode reaction process. Table 1 shows the Tafel slope of region I (β_{cI}) and region II (β_{cII}) of LDHs/6061Al and 6061Al alloys at different DO contents. Region I indicates the strong polarization stage, and region II indicates the initial reaction stage. The slope of the polarization curve of LDHs/6061Al alloy is greater than that of 6061Al alloy at different DO contents, which indicates that the resistance against the electrode reaction process of LDHs/6061Al alloy is higher than that of 6061Al alloy, because LDHs can inhibit the process of oxygen reduction. Meanwhile, for 6061Al alloy, with increasing the DO content, the slope of its polarization curve is decreased gradually. This is because the increase in DO content provides enough oxygen for the cathode reaction and accelerates the content polarization, thereby improving the cathodic reaction rate[34,35]. On the contrary, for the LDHs/6061Al alloy, the slope of its polarization curve has no significant change at different DO contents, which indicates that the existence of LDHs film prevents the DO from participating in the cathodic reaction.

In addition, there are two regions in the polarization curves of 6061Al alloy. In region II, the difference in polarization curves of 6061Al alloy at different DO contents is caused by the fact that the increase in DO content is conducive to the oxygen reduction reaction (ORR), and with ORR proceeding, the DO diffusion is not sufficient to supply the cathode consumption, which is manifested by the gradually increased Tafel slope. In region I, the difference in polarization curves results from the DO diffusion. The corrosion current density J_{corr} of 6061Al alloy is positively correlated with the DO content, because the diffusion of oxygen plays a major role in the electrochemical reaction and the cathodic reaction rate is increased with increasing the diffusion rate. The corrosion current is increased from 1.273 μA to 1.743 μA. However, the polarization behavior of LDHs/6061Al alloy is independent of the initial DO content, which indicates that LDHs film has an excellent inhibition effect against ORR.

Fig. 7 shows the anodic polarization curves of 6061Al and LDHs/6061Al alloys at different DO contents. The electrochemical parameters of 6061Al and LDHs/6061Al alloys at different DO contents were obtained by Tafel extrapolation method (Table 1). Compared with that of 6061Al alloy, the corrosion potential of LDHs/6061Al alloy is increased by 0.16 V vs. SCE on average, and its corrosion current density is significantly reduced.

The corrosion potential of 6061Al alloy shifts positively with increasing the DO content, because oxygen is a depolarizer for aluminum alloys[36]. The increase in DO content is beneficial for the formation of Al_2O_3 film, which can enhance the corrosion resistance of 6061Al alloy. Meanwhile, the corrosion current density of 6061Al alloy is increased with increasing the DO content, indicating that the increase in DO content can accelerate ORR process. However, neither the corrosion potential nor the corrosion current density of LDHs/6061Al alloy changes with increasing the DO content, indicating that LDHs/6061Al alloy has excellent insulation performance against DO.

2.4 Corrosion behavior of LDHs

Fig. 8 shows the Bode diagrams of 6061Al and LDHs/6061Al alloys in 3.5wt% NaCl solution with different DO contents. There are three and two time constants in LDHs/6061Al and 6061Al alloys, respectively. The time constants in low frequency region (10^{-2}~10^{-1} Hz) of both alloys correspond to the aluminum substrate, which is related to the electrochemical activity of the corrosion process. The time constants in the intermediate frequency region (10~10^2 Hz) of both alloys are derived from the Al_2O_3 film. The time constant in high frequency region (10^4~10^5 Hz) of LDHs/6061Al alloy is attributed to the response of LDHs/6061Al alloy film[37]. The phase angle of LDHs/6061Al alloy is larger than that of

Table 1 Cathodic polarization results of 6061Al and LDHs/6061Al alloys

Specimen	DO content/mg·L^{-1}	β_{cI}/mV·dec^{-1}	β_{cII}/mV·dec^{-1}	E_{corr}/V vs. SCE	J_{corr}/μA·cm^{-2}
6061Al	1	243.82	693.96	−0.772	1.273
	4	229.26	593.47	−0.734	1.347
	8	212.32	350.51	−0.728	1.455
	12	198.41	278.01	−0.695	1.560
	16	179.89	185.45	−0.683	1.732
LDHs/6061Al	1	264.54	-	−0.550	0.237
	4	257.06	-	−0.569	0.243
	8	250.75	-	−0.566	0.250
	12	246.36	-	−0.563	0.254
	16	239.29	-	−0.564	0.261

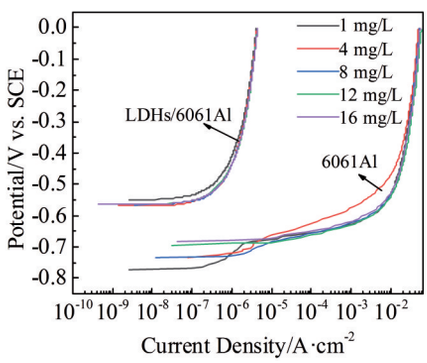

Fig.7 Anodic polarization curves of 6061Al and LDHs/6061Al alloys with different DO contents

6061Al alloy in low frequency region, indicating the high capacitance characteristics of LDHs/6061Al alloy[38,39].

Fig. 8e shows the equivalent circuit models for EIS spectra of 6061Al and LDHs/6061Al alloys. The constant phase-angle element (CPE) is used to compensate for the non-uniformity in the system instead of capacitors. The resistance of CPE is defined as $Z_{CPE}=[Y(j\omega)^n]^{-1}$, where Y is CPE constant, j is the imaginary number symbol, ω is the frequency, and n is a dimensionless index. The value of n is related to the surface heterogeneity and roughness ($0\leqslant n\leqslant 1$). If n=0, CPE means equivalent resistance; if n=1, CPE means equivalent capacitor. Besides, R_{sol} is the solution resistance of the electrolyte; CPE_{LDHs} and R_{LDHs} represent the capacitance and resistance related to the response of LDHs/6061Al alloy, respectively; CPE_{ox} and R_{ox} represent the capacitance and resistance associated with the response of the oxide film, respectively; R_{ct} and CPE_{dl} represent the charge transfer resistance and double-layer capacitance, respectively.

The fitting parameters of the equivalent circuits of 6061Al and LDHs/6061Al alloys are presented in Table 2 and Table 3,

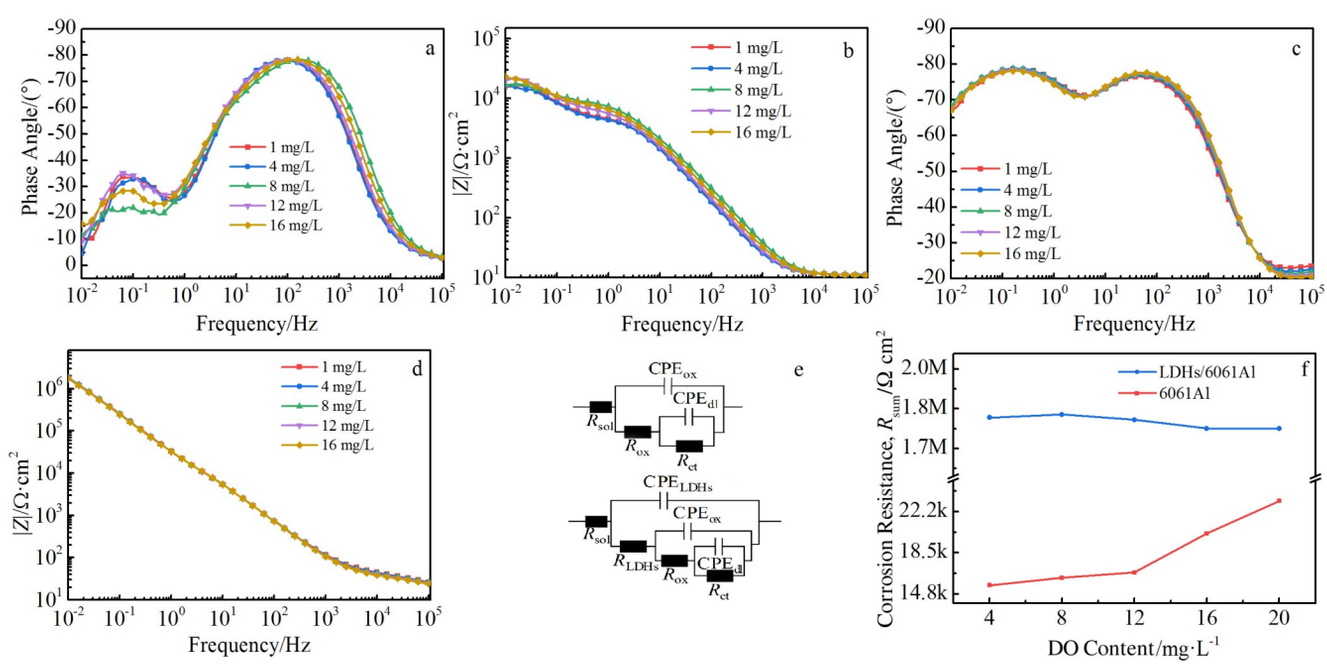

Fig.8 Bode diagrams of 6061Al (a, b) and LDHs/6061Al (c, d) alloys with different DO contents; schematic diagrams of equivalent circuit (e); relationship between corrosion resistance R_{sum} and DO content (f)

respectively. The corrosion resistance (R_{sum}) of the film is evaluated by $R_{sum}=R_{LDHs}+R_{ox}+R_{ct}$. χ^2 shows the fitting degree of the fitted circuit, and the smaller the χ^2 value, the higher the fitting degree. Fig. 8f shows the variation of R_{sum} of LDHs/6061Al and 6061Al alloys at different DO contents. The R_{sum} value of 6061Al alloy is increased slightly with increasing the DO content, resulting in the improvement of corrosion resistance. This can be attributed to the increase in R_{ox}, which is related to the formation of alumina. On the contrary, R_{sum} value of LDHs/6061Al alloy is not increased with increasing the DO content, and the R_{ox} value remains unchanged, indicating that LDHs have excellent isolation performance against DO. The corrosion resistance of LDHs/6061Al alloy is 2~3 orders of magnitude higher than that of 6061Al alloy, suggesting that LDHs film on 6061Al alloy shows better corrosion resistance. Fig.9 shows OM corrosion morphologies of 6061Al and LDHs/6061Al alloys after polarization corrosion in 3.5wt% NaCl solution with different DO contents. Under the same conditions, the corrosion degree of 6061Al alloy is obviously more serious than that of LDHs/6061Al alloy.

From the analysis of 3D corrosion morphologies in Fig.10, the corrosion degree of 6061Al alloy is increased gradually with increasing the DO content. When the DO content is 1 mg/L, the pit depth is 12 μm and area of the pits is small (Fig. 10a). When DO content is 16 mg/L, the pit depth is 19 μm. But the pits cannot be observed in LDHs/6061Al alloy at different DO contents (Fig. 10f~10j), demonstrating excellent protection of aluminum alloys.

Table 2 Fitting parameters of 6061Al alloy based on equivalent circuit

DO content/ mg·L^{-1}	CPE_{ox}/Ω^{-1}·cm^{-2}·s^{n_1}		R_{ox}/×10^3 Ω·cm^2	CPE_{dl}/Ω^{-1}·cm^{-2}·s^{n_2}		R_{ct}/×10^4 Ω·cm^2	χ^2
	Y_1	n_1		Y_2/×10^{-4}	n_2		
1	8.29×10^{-6}	0.93	4	1.18	0.91	1.02	2.15×10^{-3}
4	1.42×10^{-5}	0.80	4.87	2.50	0.95	1.16	3.41×10^{-4}
8	1.41×10^{-5}	0.92	5.14	2.34	0.95	1.23	1.58×10^{-3}
12	1.34×10^{-5}	0.91	6.51	2.02	0.90	1.74	1.09×10^{-3}
16	1.15×10^{-5}	0.91	7.08	1.95	0.74	2.08	7.84×10^{-4}

Table 3 Fitting parameters of LDHs/6061Al alloy based on equivalent circuit

DO content/ mg·L^{-1}	CPE_{ox}/Ω^{-1}·cm^{-2}·s^{n_1}		R_{LDHs}/Ω·cm^2	CPE_{dl}/Ω^{-1}·cm^{-2}·s^{n_2}		R_{ox}/×10^4 Ω·cm^2	Capacitance constant, F	R_{ct}/ ×10^6 Ω·cm^2	χ^2/×10^{-4}
	Y_1	n_1		Y_2/×10^{-6}	n_2				
1	1.16×10^{-6}	0.82	38.2	2.16	0.89	6.19	6.92×10^{-7}	1.72	5.44
4	2.05×10^{-6}	0.80	35.4	3.02	0.90	6.36	1.06×10^{-6}	1.73	6.45
8	1.97×10^{-7}	0.79	32.6	3.01	0.90	6.29	1.16×10^{-6}	1.71	5.04
12	1.89×10^{-6}	0.81	30.2	2.99	0.91	6.36	1.28×10^{-6}	1.68	3.63
16	2.37×10^{-6}	0.79	29.5	2.66	0.92	6.93	1.21×10^{-6}	1.67	4.38

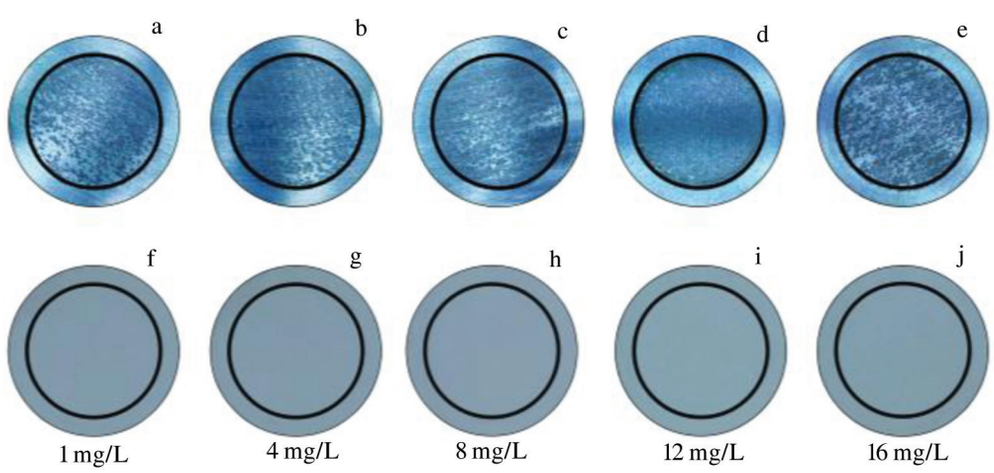

Fig.9 OM corrosion morphologies of 6061Al (a~e) and LDHs/6061Al (f~j) alloys after polarization with different DO contents: (a, f) 1 mg/L, (b, g) 4 mg/L, (c, h) 8 mg/L, (d, i) 12 mg/L, and (e, j) 16 mg/L

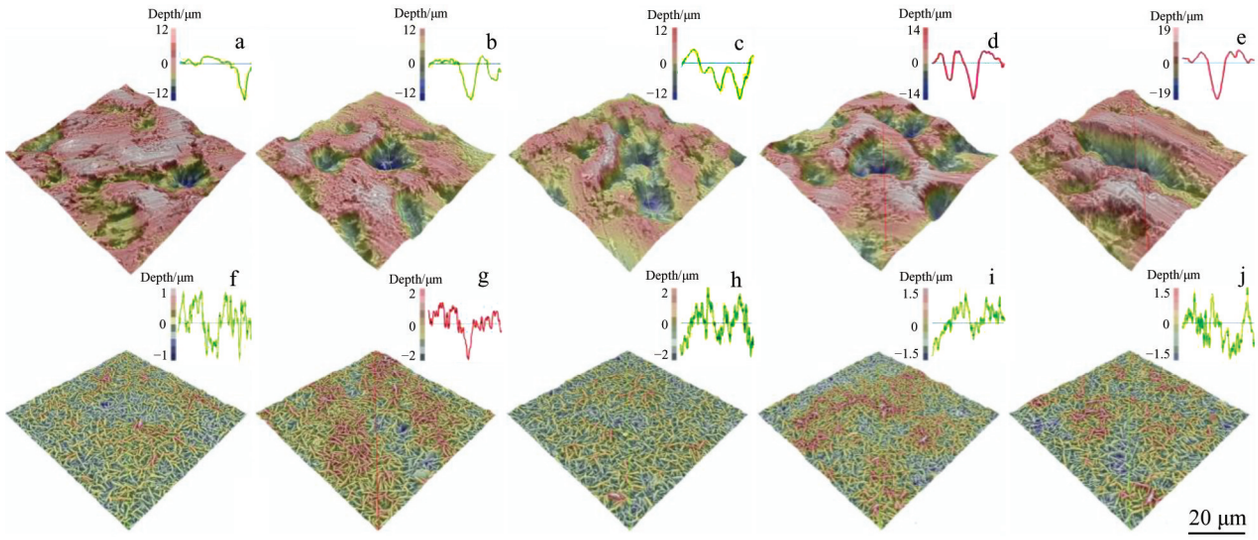

Fig.10 3D corrosion morphologies of 6061Al (a~e) and LDHs/6061Al (f~j) alloys after polarization with different DO contents: (a, f) 1 mg/L, (b, g) 4 mg/L, (c, h) 8 mg/L, (d, i) 12 mg/L, and (e, j) 16 mg/L

3 Conclusions

1) The cathodic polarization process of 6061Al and layered double hydroxides (LDHs)/6061Al alloy is controlled by the diffusion of dissolved oxygen (DO), and the polarization behavior of 6061Al alloy is also related to the initial content of DO. In the initial stage of the reaction, the increase in DO content will accelerate the reaction rate of 6061Al alloy.

2) In the strong polarization region, the cathodic reaction slope of LDHs/6061Al alloy is greater than that of 6061Al alloy at different DO contents, due to the inhibition of the cathodic polarization process caused by LDHs/6061Al alloy.

3) The LDHs film significantly enhances the corrosion resistance of 6061Al alloy, and the resistance value of LDHs/6061Al alloy is 2~3 orders of magnitude higher than that of 6061Al alloy. The resistance value of LDHs/6061Al alloy has no obvious change at different DO contents, indicating the stable protection for 6061Al alloy

4) The corrosion degree of 6061Al alloy is increased with increasing the DO content. The corrosion current is increased from 1.273 μA to 1.743 μA, and the pit depth is increased from 12 μm to 19 μm. However, the corrosion current of LDHs/6061Al alloy does not change significantly at different DO contents, and no pits can be observed.

References

1 Ji Hao, Zhang Chengyu, Qiao Shengru. *Rare Metal Materials and Engineering*[J], 2015, 44(5): 1116

2 Meng P R, Chen Y, Liu Z L. *Int J Electrochem Sci*[J], 2020, 15: 4454

3 Ezuber H, El-Houd A, El-Shawesh F. *Materials & Design*[J], 2008, 29(4): 801

4 Dexter S C. *Corrosion*[J], 1980, 36(8): 423

5 Shi L J, Song Y W, Dong K H *et al*. *Corros Sci*[J], 2021, 184: 109

6 Su H Y. *Int J Electrochem Sci*[J], 2019, 14(5): 4812

7 Kong Dejun, Wang Jinchun, Liu Hao. *Rare Metal Materials and Engineering*[J], 2016, 45(5): 1122

8 Zhang Guikai, Li Ju, Chen Chang'an *et al*. *Rare Metal Materials and Engineering*[J], 2011, 40(6): 1120

9 Zheludkevich M L, Poznyak S K, Rodrigues L M *et al*. *Corros Sci*[J], 2010, 52(2): 602

10 Ai L, Zhang C, Meng L. *J Chem Eng Data*[J], 2011, 56(11): 4217

11 Chen J, Song Y W, Shan D Y *et al*. *Corros Sci*[J], 2011, 53(10): 3281

12 Liang Siyan, Ren Weiwei, Lin Wenxin *et al*. *Rare Metal Materials and Engineering*[J], 2020, 49(8): 2830 (in Chinese)

13 Sun Junli, Li Siyuan, Xu Hengxu *et al*. *Rare Metal Materials and Engineering*[J], 2020, 49(12): 4237 (in Chinese)

14 Poznyak S K, Tedim J, Rodrigues L M *et al*. *ACS Appl Mater Inter*[J], 2009, 1(10): 2353

15 Pavel O, Stamate A E, Bacalum E *et al*. *Catalysis Today*[J], 2021, 366: 227

16 He S, Zhao Y F, Wei M *et al*. *Ind Eng Chem Res*[J], 2011, 50(5): 2800

17 Han J B, Xu X Y, Rao X Y *et al*. *J Mater Chem*[J], 2011, 21(7): 2126

18 Guo X X, Xu S L, Zhao L L *et al*. *Langmuir*[J], 2009, 25(17): 9894

19 Yarger M S, Steinmiller E M P, Choi K S. *Inorg Chem*[J], 2008, 47(13): 5859

20 Wu F X, Liang J, Peng Z J *et al*. *Appl Surf Sci*[J], 2014, 313: 834

21 Truesdale G A, Downing A L, Lowden G F. *Journal of Applied Chemistry*[J], 1955, 5(2): 53

22 Reinhart F M. *Corrosion of Materials in Hydrospace-Part V-Aluminum Alloys*[R]. Hueneme: Naval Civil Engineering Lab Port, 1969
23 Jaiswal A, Mani R, Banerjee S *et al*. *J Mol Liq*[J], 2015, 202: 52
24 Lajevardi S, Mosalaeepour L, Shahrabi T. *Corros Eng Sci Technol*[J], 2010, 45(4): 295
25 Cao Y H, Dong S G, Zheng D J *et al*. *Corros Sci*[J], 2017, 126: 166
26 Song F, Hu X L. *Nat Commun*[J], 2014, 5: 4477
27 Salak A N, Lisenkov A D, Zheludkevich M L *et al*. *ECS Electrochem Lett*[J], 2013, 3(1): 9
28 Huang Q Y, Wang Y B, Zhou B T *et al*. *Corros Sci*[J], 2021, 179: 109 165
29 Pan D K, Zhang H, Zhang T *et al*. *Chem Eng Sci*[J], 2010, 65(12): 3762
30 Liu Z P, Ma R Z, Osada M *et al*. *J Am Chem Soc*[J], 2006, 128(12): 4872
31 Sjastad A O, Andersen N H, Vajeeston P *et al*. *Eur J Inorg Chem*[J], 2015, 2015(10): 1775
32 Yasaei M, Khakbiz M, Ghasemi E *et al*. *Appl Surf Sci*[J], 2019, 467-468: 782
33 Zuo Y, Zhao P H, Zhao J M. *Surf Coat Technol*[J], 2003, 166(2-3): 237
34 Melchers R E. *Corros Eng Sci Technol*[J], 2006, 41(1): 38
35 Melchers R E, Jeffrey R. *Corros Sci*[J], 2005, 47(7): 1678
36 Pauli J, Sobolik V, Onken U. *Chem Eng Sci*[J], 1991, 46(12): 3302
37 Wang Y B, Zhang Y S, Zhou B T *et al*. *Materials & Design*[J], 2019, 180: 107 952
38 Wang Z B, Hu H X, Liu C B *et al*. *Electrochimic Acta*[J], 2014, 135: 526
39 Gonzalez J E G, Mirza-Rosca J C. *J Electroanal Chem*[J], 1999, 471(2): 109

LDHs对6061铝在不同溶解氧浓度的NaCl溶液中腐蚀行为的影响

袁增崟[1,2]，王友彬[1,2]，邹　睿[1,2]，杨元成[1,2]，藤田丰久[1,2]，韦悦周[1,2]
(1. 广西有色金属及特色材料加工重点实验室，广西 南宁 530004)
(2. 广西大学 资源环境与材料学院，广西 南宁 530004)

摘　要：通过原位合成法在6061Al合金表面制备了层状双氢氧化物（LDHs），使用极化曲线（Tafel）和电化学阻抗谱（EIS）研究了在3.5%（质量分数）NaCl溶液中不同溶解氧浓度（1~16 mg/L）下LDHs对6061Al合金腐蚀行为的影响。结果表明，6061Al合金与LDHs/6061Al合金的极化过程均受到溶解氧的扩散控制。随着溶解氧浓度的增加，6061Al合金的腐蚀更加剧烈，其腐蚀电流由1.273 μA增加到了1.743 μA，蚀坑深度由12 μm增加到了19 μm。而LDHs/6061Al合金在各溶解氧浓度下均未观察到蚀坑，这是由于LDHs薄膜阻碍了溶解氧的扩散，其极化过程受到了抑制。此外，随着溶解氧浓度的增加，6061Al合金的阻抗显著增加，这与Al_2O_3的形成有关；而LDHs/6061Al合金的阻抗在不同溶解氧浓度下未发生明显变化，表现出对溶解氧优异的隔绝性能。

关键词：LDHs；溶解氧；铝合金；腐蚀

作者简介：袁增崟，男，1995年生，硕士生，广西大学资源环境与材料学院，南宁 广西 530004，E-mail：yuanzengyin@126.com